Contents list available at CBIORE journal website

International Journal of Renewable Energy Development

Journal homepage: https://ijred.cbiore.id

Research Article

Performance and emissions of a diesel engine fuelled with ultrasonically produced tobacco seed oil methyl ester: An RSM optimization study

Binh Vu Duc[a], Van Vuong Nguyen[a], Du Nguyen[b], Thanh Hai Truong[c,*]

[a]*Faculty of Mechanical and Automotive Engineering, Viet Tri University of Industry, Phu Tho, Vietnam*

[b]*Institute of Engineering, HUTECH University, Ho Chi Minh City, Viet Nam*

[c]*PATET Research Group, Ho Chi Minh City University of Transport, Ho Chi Minh City, Viet Nam*

Abstract. Biodiesel plays an important role in making diesel engines more environmentally friendly and sustainable. Biodiesel use can significantly lower emissions of harmful pollutants, contributing to cleaner air and a reduced impact on climate change. Although there is an increasing body of research on non-edible biodiesel feedstocks, few studies have been able to systematically correlate fuel production, blend variation, and engine load optimization with a single statistical framework. This study fills this gap by combining ultrasonic-assisted two-step transesterification of tobacco seed oil (TSO) with response surface methodology to determine engine performance and emissions. Acid esterification was performed to produce TSO methyl ester, which was subjected to transesterification with NaOH under ultrasonic irradiation, to guarantee efficient conversion and low levels of free fatty acids. Indeed, TSO biodiesel and diesel fuel blends were tested on the engine under different loads. The findings indicate that the engine has a critical operating point of Engine Load (EL) = 96.90% and Lower Heating Value (LHV) = 41.82 MJ/kg, at which the engine has a peak thermal performance with BTE = 32.98% and BSFC = 0.27 kg/kWh. This indicates a very effective conversion of energy because of high in-cylinder temperature and pressure. Additionally, CO and HC emissions are significantly reduced, meaning that the combustion is almost complete. Nevertheless, NOx emissions increase dramatically to 657.74 ppm, proving the thermal penalty of high-temperature operation. This trade-off is validated by multi-objective optimization, which offers a strong framework to balance efficiency and emissions in biodiesel-powered engines.

Keywords: Alternative fuel; Sustainability; Biodiesel; Tobacco Seed Biodiesel; ANOVA; Optimization

Received: 18th Feb 2026; Revised: 3rd May 2026; Accepted: 27th May 2026; Available online: 10th June 2026

1. Introduction

The accelerated exhaustion of the world's fossil fuel reserves, coupled with the growing environmental issues associated with greenhouse gas emissions and deterioration of air quality, has heightened the quest to seek viable renewable energy sources (Alsaadi *et al*., 2025; T. T. Le *et al*., 2024). It takes about 580 TJ of energy to satisfy the world's demand, about 80% of which is provided by burning conventional fossil fuels, a trend that is still increasing the rate at which non-renewable reserves are being depleted (Kober *et al*., 2020). Biodiesel has become one of the most promising alternatives to petroleum-based diesel, due to its renewability, biodegradability, and ability to be used in the existing diesel engines without structural adjustments (Desniorita *et al*., 2026; Huynh *et al*., 2025; V. G. Nguyen *et al*., 2024). Regular diesel engines can operate on biodiesel without any alterations, and engine performance is not greatly affected when biodiesel is used as an alternative fuel (Gang *et al*., 2025; Hoang, 2021; Sharma & Sharma, 2022). Moreover, its naturally elevated oxygen content facilitates more complete combustion, minimizes the harmful tailpipe emissions, and its insignificant sulfur content assists in avoiding the development of sulfur oxide pollutants (John *et al*., 2026; Rahman *et al*., 2026; Zafar *et al*., 2026). In recent times, many countries have mandated the use of biodiesel-diesel blends for road as well as marine transport (Wei *et al*., 2024).

The nature of the feedstock of biodiesel is a critical determinant of its long-term viability. First-generation biodiesel made of edible vegetable oils (soybean, palm, and rapeseed) is a major cause of concern in terms of food security, arable land utilization, and economic competition with the food supply chain (Christopher Selvam *et al*., 2026; K. B. Le *et al*., 2026; Prajapati *et al*., 2026). Non-edible feedstocks like Jatropha and algae provide great benefits as they reduce food-security issues and, at the same time, allow high biodiesel production due to effective catalytic reactions (Szulczyk & Badeeb, 2022; Yew *et al*., 2019). One of these non-edible feedstocks with a lot of potential is tobacco seed oil (TSO). Tobacco farming produces huge amounts of agricultural byproducts in the form of tobacco seeds, which are not utilized by humans, and TSO is a rich and economically viable raw material in biodiesel production (Fornasier *et al*., 2018; Tian *et al*., 2021; Usta *et al*., 2011; Veljković *et al*., 2006). Although this is possible, studies that specifically examine the use of tobacco seed oil methyl ester (TSOME) as a fuel in diesel engines are relatively few, especially in terms of how to optimize engine operating conditions at

* Corresponding author(s):
Email: hai.truong@ut.edu.vn (T.H. Truong)

https://doi.org/10.61435/ijred.2026.62705
ISSN: 2252-4940/© 2026.The Author(s). Published by CBIORE

various blend ratios and loads (Donatus Setyawan Purwo Handoko, 2022; Quaranta *et al*., 2022). The most common method of biodiesel production is the transesterification process, where triglycerides in vegetable oil are transformed to fatty acid methyl esters (FAMEs) in the presence of an alcohol and a catalyst (Awogbemi *et al*., 2020; Shrivastava *et al*., 2021). Kalyani et al. (Kalyani *et al*., 2023) used RSM to optimize the biodiesel production from algae spirogyra, helping to achieve a biodiesel yield of 96.18%. Kolakoti et al. (Kolakoti *et al*., 2022) also used RSM and moringa leaves as a catalyst to achieve a biodiesel yield of 92.82%. Nonetheless, the natural immiscibility of the oil and alcohol phases poses a basic mass transfer constraint that negatively impacts reaction efficiency, yield, and energy usage in traditional mechanically stirred (Zullaikah *et al*., 2021). Onokowai et al. (Onokowai *et al*., 2025) employed RSM to optimize bio-oil yield from Cocos nucifera through the pyrolysis process. The maximum bio-oil yield (52.2 wt.%) was achieved at a temperature of 510.2°C, with heating rates of 10.5°C/min, a residence duration of 5.2 minutes, a particle size of 0.3, and a nitrogen flow rate of 17.3 mL/min. As a process intensification method, ultrasonic irradiation increases agitation between immiscible reactants, uniform heating by localized temperature rises, and creation of microjets by the temporary collapse of cavitation bubbles, thus greatly decreasing energy usage (Oza *et al*., 2021; Sebayang, Ideris, *et al*., 2023). Use of ultrasonic energy in the production of biodiesel has been supported as an effective method that enhances mass transfer between phases of reactants, leading to reduced reaction time and possibly reduced cost of the process (Di *et al*., 2009). The ultrasound-assisted transesterification studies have continually shown significant reaction time reductions over the traditional methods (Mujtaba *et al*., 2020). Ultrasonic irradiation has been demonstrated to decrease the time of transesterification reaction to as short as 5 minutes under normal heating conditions, yet with similar yields of biodiesel, and has also been reported to enhance the physicochemical characteristics of the resulting biodiesel, such as lower density and viscosity (Riayatsyah *et al*., 2021; Sebayang, Kusumo, *et al*., 2023). Sodium hydroxide (NaOH) was chosen as the base catalyst in the transesterification step in the current study. Previous studies on cottonseed oil have reported methyl ester yields of up to 98 wt.% under ultrasonic irradiations of NaOH at 1 wt.% relative to the mass of oil and a 6.2:1 molar ratio of methanol to oil (Ahmad *et al*., 2024; Prakash Maran & Priya, 2015; Sarve *et al*., 2015).

After the production, biodiesel is usually mixed with petroleum diesel in different volumetric proportions before engine testing. Two of the most significant variables that determine the performance and emission properties of a CI engine fuelled with biodiesel blends are the engine load and blend concentration (Hoang, Nayak, *et al*., 2025; Nayak *et al*., 2022; Sharma *et al*., 2022). Experiments on diesel engines that are fuelled by biodiesel-diesel mixtures have revealed that brake thermal efficiency declines with the proportion of biodiesel in the fuel because of the reduced calorific value of biodiesel, whereas NOx emissions tend to rise and CO emissions tend to fall at higher blend ratios and full load (Ahmad *et al*., 2025; Teklehaimanot *et al*., 2025; Vellaiyan, 2025). In research with pumpkin methyl ester blends, 20, 40, and 60 percent biodiesel blends were tested at full engine load ranges under RSM to maximize brake thermal efficiency and minimize brake-specific fuel consumption, NOx, CO, smoke, and hydrocarbon emissions (Kuppuswami *et al*., 2024). These results demonstrate the multifaceted, frequently complex trade-offs between performance benefits and emission penalties that require an organized optimization framework (Hoang, Chen, *et al*., 2025).

Response Surface Methodology (RSM) has become a popular statistical method used in biodiesel engine studies as a powerful statistical tool in the simultaneous optimization of various engine response variables (Shami et al., 2023). RSM is widely applied in biodiesel research to optimize fuel formulations, to assess the impact of various production processes on biodiesel properties, and to predict the performance and emission properties of diesel engines (Khandal *et al*., 2024; Lv *et al*., 2024; Rajak *et al*., 2024; Susaimanickam *et al*., 2023). The RSM-based studies generally use central composite or Box-Behnken designs to describe the correlation between input factors, including blend ratio, engine load, injection pressure, and compression ratio, and responses, including brake thermal efficiency (BTE), brake-specific fuel consumption (BSFC), and exhaust gas emissions. The correlation coefficients (R^2) of engine performance and emission responses are between 0.9785 and 0.9997 with RSM-derived regression models, which indicates the high predictive power of the methodology when used to predict biodiesel-fuelled diesel engine systems (Muniyappan & Krishnaiah, 2025; Ouchikh *et al*., 2025; Ugraram, 2025; Zhang *et al*., 2025). Although there is an increasing literature on non-edible biodiesel feedstocks and their uses in engines, there are still some important gaps. Although tobacco seed oil is a relatively new feedstock of interest, the current research on TSOME has been more concerned with optimization of the transesterification production process itself and the impact of hybrid nanoparticle additives on engine performance, as opposed to a systematic study of the overall impact of the blend ratio and engine load on the performance and emission parameters of the engine using a systematic statistical optimization strategy. In addition, previous studies on ultrasound-assisted biodiesel production using new seed oils have also pointed out the gap in research specifically relating the ultrasonic production process to downstream engine performance analysis, with a lack of information on the use of ultrasonically produced biodiesel in diesel engines under various operating conditions. Importantly, none of the studies so far have integrated ultrasonic-assisted two-step transesterification of tobacco seed oil with RSM-based optimization of engine performance and emission parameters at various blend ratios and load levels concurrently. Most of the available literature either assesses one concentration of biodiesel blend, or operates at a constant engine load, or uses optimization methods without considering the interaction effects between blend percentage and engine load - a limitation that restricts the real-world applicability of their results to engine operation.

To address these identified gaps, the present study aims to: (1) produce TSOME via an ultrasonic-assisted two-step transesterification process employing acid-catalyzed esterification followed by NaOH-catalyzed base transesterification; (2) evaluate the performance characteristics — including BTE, BSFC and emission profiles including CO, NOx, HC, and smoke opacity — of a single-cylinder CI diesel engine fuelled with TSOME-diesel blends (B10, B20, B30, and B40) across varying engine loads (10 to 100%); and (3) apply Response Surface Methodology to develop predictive regression models and identify optimal combinations of blend ratio and engine load that simultaneously maximize engine performance while minimizing harmful exhaust emissions. This study is likely to provide practically actionable information on the feasibility of TSOME as a sustainable diesel alternative and a reproducible statistical framework for other non-edible seed oil biodiesels.

2. Materials and methods

2.1 Test biofuel

The biodiesel investigated in this study was produced from tobacco seed oil, a non-edible and readily available raw material. Given that the unrefined tobacco seed oil exhibited elevated free fatty acid (FFA) concentrations, a sequential two-stage process was employed to synthesize tobacco seed oil methyl ester (TSOME). The first stage involved acid-catalyzed esterification to reduce FFA levels. Methanol and concentrated sulfuric acid (H_2SO_4) were introduced into the crude oil at a molar ratio of 6:1 (methanol to oil), with H_2SO_4 constituting 1% v/v as the catalyst. The lab scale test setup is illustrated in Fig. 1 (Chamkalani *et al*., 2020; Sakthivel *et al*., 2018). To enhance interfacial contact between the immiscible phases, the reaction mixture was subjected to ultrasonic irradiation at 40 kHz using a probe-type ultrasonicator, maintained at 55°C for 60 minutes. This approach successfully reduced FFA content from approximately 4.8% to below 1.0%, meeting the threshold required for subsequent alkaline-catalyzed conversion. The esterified oil was recovered by allowing the mixture to settle and extracting the upper phase. The second stage consisted of base-catalyzed transesterification using sodium hydroxide (NaOH) as the catalyst. NaOH at 1% w/w relative to oil mass was dissolved in methanol and combined with the pre-treated oil, maintaining a 6:1 methanol-to-oil molar ratio (Naseef & Tulaimat, 2025; Wan Osman *et al*., 2024). The reaction mixture was subjected to ultrasonic irradiation at 40 kHz at 60°C for 40 minutes, with cavitation-induced micro-mixing facilitating efficient conversion of triglycerides to fatty acid methyl esters. Upon completion, the product was transferred to a separating funnel and allowed to gravity-separate over 24 hours, yielding a biodiesel-rich upper layer and a glycerol-rich lower phase. The crude biodiesel was purified through repeated warm deionized water washes to eliminate residual catalysts, saponified byproducts, and unreacted methanol, continuing until a neutral pH was achieved. Residual moisture was subsequently removed by oven-drying the sample at 105°C for two hours. The final TSOME product was stored in sealed containers before blending and characterization. The main properties of test fuel blends are listed in Table 1.

2.2 Test Engine and Dynamometer

The experimental investigations were conducted using a computerized single-cylinder, four-stroke, water-cooled, direct injection (DI) diesel engine test rig. The engine coupled to the test rig was a Kirloskar TV1 model, a widely employed research-grade engine owing to its robustness and well-documented performance characteristics. The engine operated at a constant speed of 1500 rpm and delivered a rated power output of 5.2 kW (7 BHP). The key geometric specifications of the engine included a bore diameter of 87.5 mm, a stroke length of 110 mm, a swept volume of 661 cc, and a compression ratio of 17.5:1. Engine loading was achieved using a water-cooled eddy current dynamometer (Model AG10) coupled to the engine via a propeller shaft with universal joints. The dynamometer loading unit (Model AX-155) operated on a constant-speed supply of 230V AC, enabling precise and stepwise variation of engine load. The main specifications of the test engine setup are listed in Table 2. A schematic representation of the test setup is depicted in Fig. 2. Experiments were conducted from low engine load to full engine load to comprehensively evaluate the

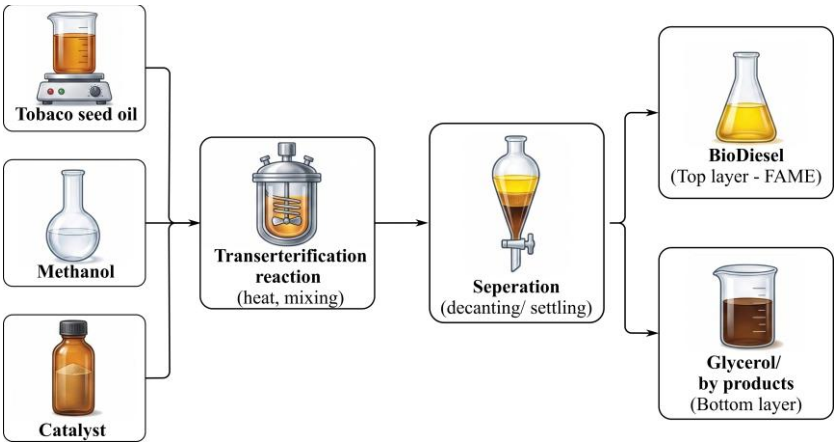

Fig 1. Biodiesel synthesis setup

Table 1
Physicochemical Properties of Test Fuels and Applicable ASTM Standards

Property	Test method	Diesel (B0)	TSO-based biodiesel (B100)	B10	B20	B30	B40	ASTM limit
Density at 15°C (kg/m³)	D4052	835	876	839	843	848	854	860–900
Kinematic viscosity at 40°C (mm²/s)	D445	2.8	4.2	3.0	3.2	3.5	3.7	1.9–6.0
Flash point (°C)	D93	68	162	74	81	95	108	Min. 130
Lower heating value (MJ/kg)	D240	43.0	38.8	42.6	42.0	41.4	40.8	—
Cetane number	D613	50	71	52	54	57	59	Min. 47
Cloud point (°C)	D2500	−12	−2	−11	−9	−7	−5	—
Pour point (°C)	D97	−18	−6	−17	−15	−12	−9	—

Table 2
Specifications of the Kirloskar TV1 Engine Test Setup

Parameter	Specification
Engine Make and Model	Kirloskar TV1
Engine Type	Single cylinder, 4-stroke, DI Diesel
Cooling System	Water cooling
Rated Power	5.2 kW (7 BHP) at 1500 ± 50 rpm
Bore × Stroke	87.5 mm × 110 mm
Displacement Volume	661 cc
Compression Ratio	17.5:1
Operating Speed	1500 rpm (constant)
Dynamometer Type	Eddy current, water-cooled
Dynamometer Model	SAJ Test Plant, Model AG10
Piezo Sensor Range	5000 PSI
Crank Angle Sensor Resolution	1° with TDC pulse
Data Acquisition Device	NI USB-6210, 16-bit, 250 kS/s
Fuel Tank Capacity	15 litres

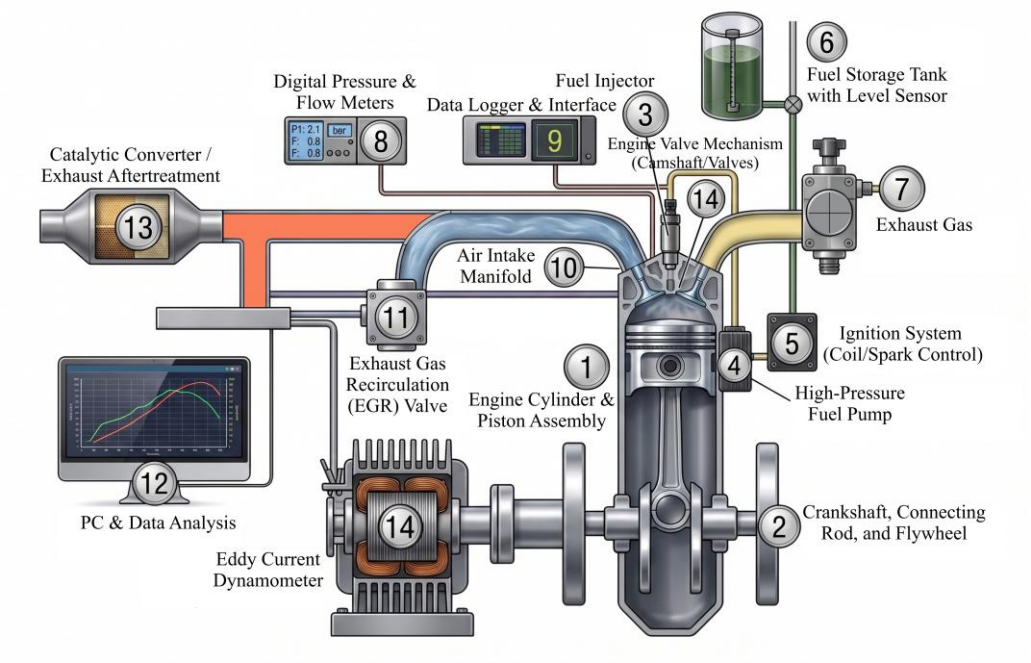

Fig 2. Test setup

influence of load variation on engine performance and emission responses across all tested fuel blends.

2.3 Instrumentation and Data Acquisition

The test setup was equipped with a comprehensive array of instruments for the real-time measurement and recording of combustion, performance, and thermal parameters. In-cylinder combustion pressure was measured using a piezoelectric pressure sensor with a range of 5000 PSI, connected via a low-noise coaxial cable to minimize signal interference. Crank angle measurement was performed using a dedicated crank angle sensor with a resolution of 1 degree and a maximum operating speed of 5500 RPM, incorporating a top dead centre (TDC) pulse for precise phase referencing. These two signals were processed together to generate pressure–crank angle (P-θ) and pressure–volume (P-V) indicator diagrams via an engine indicator interface connected to a computer.

Airflow to the engine was measured using an MS-fabricated air box fitted with an orifice meter and a U-tube manometer (Model MX-104, Apex Innovations; range ±100 mm). Fuel flow rate was quantified using a calibrated glass fuel metering column integrated within a 15-litre capacity fuel tank. Cooling water and calorimeter water flow rates were monitored using two Eureka rotameters (Models PG5 and PG6; ranges 25–250 lph and 40–400 lph, respectively). Temperature measurements at multiple points, including engine jacket inlet and outlet, calorimeter inlet and outlet, and exhaust gas, were acquired using PT100 RTD sensors and Type-K thermocouples connected to two-wire temperature transmitters (range 0–100°C, output 4–20 mA). All analog signals were digitized and processed through a National Instruments data acquisition device (NI USB-6210 and 16-bit resolution), interfaced with the Engine Soft software platform, a LabVIEW-based engine performance monitoring system developed by Apex Innovations.

2.4 Uncertainty analysis

In any experimental study that uses several measuring instruments and the resulting calculated parameters, there must be a systematic evaluation of the measurement uncertainty in order to justify the reliability and credibility of the results reported. Sources of error in experimental data may be of two main origins: instrument errors, due to the accuracy class and

resolution of the measuring instruments, and human error, which may be caused by reading, recording, or operating the equipment. Despite the carefulness and caution that are observed during the experiment, certain errors might be accidentally caused by the experimental nature of the work. To measure and report such errors, the uncertainty analysis was conducted in the current study based on the approach suggested by Kline and McClintock, which is commonly used in engine performance and emission studies (Kline & McClintock, 1953).

Root-sum-square method to compute the percentage uncertainty in any quantity R derived as a function of several independent measured variables (x1, x2, x3, xn) is given as:

$$W_R = \sqrt{[\,(\partial R/\partial x_1 \cdot w_1)^2 + (\partial R/\partial x_2 \cdot w_2)^2 + \ldots + (\partial R/\partial x_n \cdot w_n)^2\,]} \quad (1)$$

W_R is the overall uncertainty in the result R, and w1, w2,...wn are the respective uncertainties of each measured variable. The instruments employed in the experimental system have a given manufacturer-specified accuracy, and the uncertainty of each directly measured parameter, such as load, speed, fuel consumption, temperatures, and airflow, was calculated using the values of the accuracy.

The main performance parameters calculated in this paper are brake power (BP), brake-specific fuel consumption (BSFC), and brake thermal efficiency (BTE), each are calculated based on various measured quantities and thus combines uncertainty due to each measurement that contributes to them. Brake power is a product of dynamometer torque and engine speed; BSFC is formed of the rate of mass flow of fuel and brake power, and BTE also relies on the lower heating value (LHV) of the test fuel. The spread of individual instrument uncertainties by these interdependent forms gives the cumulative percentage uncertainty of each calculated parameter. Table 3 summarizes the instruments employed, their measurement ranges, their accuracy classes, and the percentage uncertainty associated with them.

2.5 Response Surface Methodology

Response Surface Methodology (RSM) is a statistical and mathematical method of modeling, analyzing, and optimizing a process in which a response is influenced by multiple input variables (Hoang, Bora, *et al.*, 2025). It is particularly applicable to cases where there are several factors that interact in a complex and nonlinear fashion, such that classical experimentation is inefficient or incomplete (D. Nguyen *et al.*, 2025; T. H. Nguyen *et al.*, 2024). RSM is performed by establishing an empirical correlation among the input variables and the response output, which can be expressed as a second-order polynomial equation (Sarabia & Ortiz, 2009). This enables researchers to estimate the actual functional relationship in a specified area of an experiment. RSM is able to capture individual and interaction effects by systematically varying input parameters, giving a better insight into system behavior. The approach also allows the creation of response surfaces and contour plots, which can be used to visualize the effects of variable variations on the outcome (Djimtoingar *et al.*, 2022; V. N. Nguyen *et al.*, 2023). These visual aids are useful in determining the best conditions to maximize or even minimize the desired response. RSM is also commonly used in engineering, manufacturing, energy systems, and biotechnology to optimize processes and increase performance (Dong & Sharma, 2023; Paramasivama *et al.*, 2024). It also aids sensitivity analysis and is useful in establishing which variables are most important in the response (Gunst *et al.*, 1996). Python-based scientific computing libraries, including NumPy, Pandas, Matplotlib, Seaborn, and Statsmodels, were employed for RSM in this study. In general, RSM provides a viable trade-off between experimental and modeling performance and is an effective tool in the optimization of complex systems with resource and time limitations.

3. Results and discussion

3.1 Analysis of variance

The results of ANOVA can be strictly interpreted by relating the statistical magnitudes to the physics of combustion, EL is engine load, and LHV is fuel lower heating value, which directly regulate the rate of energy release, in-cylinder temperature, and oxidation process. In the case of brake thermal efficiency (Table 4), EL shows an overwhelming dominance with a sum of squares of 874.17, a very large F value of 33900.88, and a p-value of 1.40×10^{-5} that shows clearly that changes in load are the dominant factor in the energy conversion process. Physically, a rise in EL increases the volume of fuel injected and in-cylinder pressure, which results in higher peak temperatures and better combustion efficiency as the expansion stroke is better utilized and relative heat losses are minimized. By contrast, LHV has a

Table 3
Precision and Measurement Uncertainty of Measuring Devices

Parameter/instrument	Range	Precision	Uncertainty (%)
Engine speed (crank angle sensor)	0–5500 rpm	±1 rpm	±0.15
Load (load cell/dynamometer)	0–20 kgf	±0.1 kgf	±0.20
Fuel flow (glass burette column)	0–100 mL	±0.1 mL	±0.31
Airflow (orifice + manometer)	0–100 mm H_2O	±1 mm	±0.25
Temperature (PT100 RTD sensor)	0–100°C	±0.5°C	±0.18
Temperature (type-K thermocouple)	0–1200°C	±1°C	±0.20
In-cylinder pressure (piezo sensor)	0–350 bar	±1 bar	±0.35
Emission parameters			
CO emission (gas analyser)	0–10% vol	±0.02%	±0.50
HC emission (gas analyser)	0–20000 ppm	±10 ppm	±0.55
NOx emission (gas analyser)	0–5000 ppm	±10 ppm	±0.60
Computed parameters			
Brake power	—	—	±0.21
Fuel consumption	—	—	±0.31
BSFC	—	—	±0.52
BTE	—	—	±1.82

Table 4.
ANOVA for BTE and BSFC

Response	BTE (%)			BSFC (kg/kWh)		
Factor	sum_sq	F	PR(>F)	sum_sq	F	PR(>F)
x1	874.17	33900.88	1.40E-52	0.1055	11370.67	1.58E-44
x2	37.17	1441.37	2.00E-29	0.0211	2275.93	9.77E-33
I(x1*x1)	13.49	523.20	3.15E-22	0.0029	308.87	1.24E-18
I(x2*x2)	1.46	56.76	9.52E-09	0.0005	55.29	1.26E-08
x1:x2	0.31	11.86	0.0015	0.0004	45.23	1.00E-07
Residual	0.88			0.0003		

Table 5
ANOVA for NOx, CO, and HC emissions

	NOx (ppm)			CO (%)			HC (ppm)		
Factor	**Sum sq**	**F**	**PR(>F)**	**Sum sq**	**F**	**PR(>F)**	**Sum sq**	**F**	**PR(>F)**
x1	721001.89	5403.57	4.65E-39	0.03	2934.8	1.37E-34	1553.50	8042.39	5.58E-42
x2	30319.69	227.23	1.28E-16	0.0019	182.8	3.09E-15	93.89	486.09	1.02E-21
I(x1*x1)	464.06	3.48	0.07	0.0004	40.01	3.27E-07	0.55	2.83	0.1014
I(x2*x2)	199.75	1.50	0.229	0.00002	1.53	0.22	1.46	7.54	0.0095
x1:x2	391.57	2.93	0.096	0.0003	26.38	1.14E-05	2.51	12.97	0.0009
Residual	4536.64			0.00037			6.57		

*Here, x1 denotes engine load while x2 denotes LHV of fuel blend.

significantly lower number of squares of 37.17 and the F-value of 1441.37, which is approximately 4% of the variation when compared to EL, which indicates its secondary role in predicting the intrinsic energy content of the fuel and the temperature and burning velocity of the flame. The quadratic effect of EL, whose sum of squares is 13.49 and F value is 523.20, is a nonlinear effect due to thermodynamic constraints, including more heat transfer losses and potential dissociation at higher loads, whereas the smaller quadratic effect of LHV is a confirmation of weaker curvature in its effect. In the case of brake specific fuel consumption (Table 4), EL is once again the leading factor with a sum of squares of 0.1055 with an F value of 11370.67, indicating that the fuel consumption is very sensitive to load since the higher EL, the better thermal efficiency, and the less fuel needed to produce a unit power output. LHV has a 0.0211 contribution with an F value of 2275.93, meaning that more energy content in the fuel reduces the fuel mass required, but the impact is not more important than the load. In the case of nitrogen oxides, EL indicates a huge sum of squares of 721001.89 and an F value of 5403.57, which indicates that the formation of NOx is highly controlled by load because of its influence on the peak combustion temperature and oxygen availability, in line with the thermal NO formation mechanism. LHV adds 30319.69 or approximately 4 % of the EL contribution, meaning that increased heating value fuels slightly increase flame temperature and consequently NOx, but the primary cause is load. The F values of the quadratic and interaction terms of NOx are comparatively low, e.g., 3.48 of EL squared with a p-value of 0.07, which indicates that these two variables are almost linear in the range of the study (Table 5). In the case of carbon monoxide, EL once again prevails with a sum of squares of 0.03 and an F value of 2934.8, with LHV adding 0.0019 with an F value of 182.8, indicating that incomplete combustion is largely affected by load due to its ability to control air-fuel equivalence ratio and oxidation time. The large quadratic contribution to EL on CO, F 40.01, and p-value 3.27 x 10^7, indicates nonlinear behavior in which the low and very high loads may raise CO because of inadequate mixing or oxidation time. In the case of hydrocarbons, the sum of squares of EL is 1553.50, and the F value is 8042.39, versus 93.89 and 486.09 in the case of LHV, which implies that the EL has a stronger explanatory power than LHV. This implies that the unburned hydrocarbons are very sensitive to load because of flame quenching, crevice, and partial combustion at non-optimal conditions. The interaction value of hydrocarbons of 12.97 and p-value of 0.0009 confirm that the interaction of EL and LHV has an impact on flame propagation and oxidation completeness. All in all, the quantitative data indicate that EL is the main controlling factor in all responses, with LHV serving as a secondary thermochemical factor, and the very small residual values indicate that the statistical model is successful at governing combustion physics.

3.2 RSM-based contour plots and surface diagrams

3.2.1 Brake-thermal efficiency model

Fig. 3 and Fig. 4 show the interaction of EL and LHV on BTE and BSFC in contour and three-dimensional surface plots, which allow a clear visualization of the controlling thermodynamic trends. Fig. 3a, the contour plot of BTE, indicates that the efficiency is strongly positive along the EL axis, with efficiency increasing to over 3133% at high EL (near full load) and efficiency decreasing to almost 16 to 18% at low EL (near 10). This sharp gradient proves that EL is the prevailing factor affecting efficiency, as also shown by the closely spaced contour lines in the horizontal direction. The rise in BTE is relatively moderate along the LHV axis, with the percentage of increase in BTE increasing between about 22 and 29 percent between 39.5 MJ/kg and 41.5-42 MJ/kg with a fixed EL of approximately 60%, indicating that higher fuel energy content increases combustion temperature and heat release but with a lesser effect than load. The nonlinearity is mildly indicated by the curvature of contour lines, particularly at higher EL, where BTE gains start to level off (K. B. Le *et al.*, 2026). This observation is further supported by Fig. 3b, which shows that BTE increases rapidly with EL and more slowly with LHV, peaking at about 3233% at EL near 100% and LHV near 42 MJ/kg. There is also a slight bending at high EL on the surface, which means that there are diminishing returns as the heat

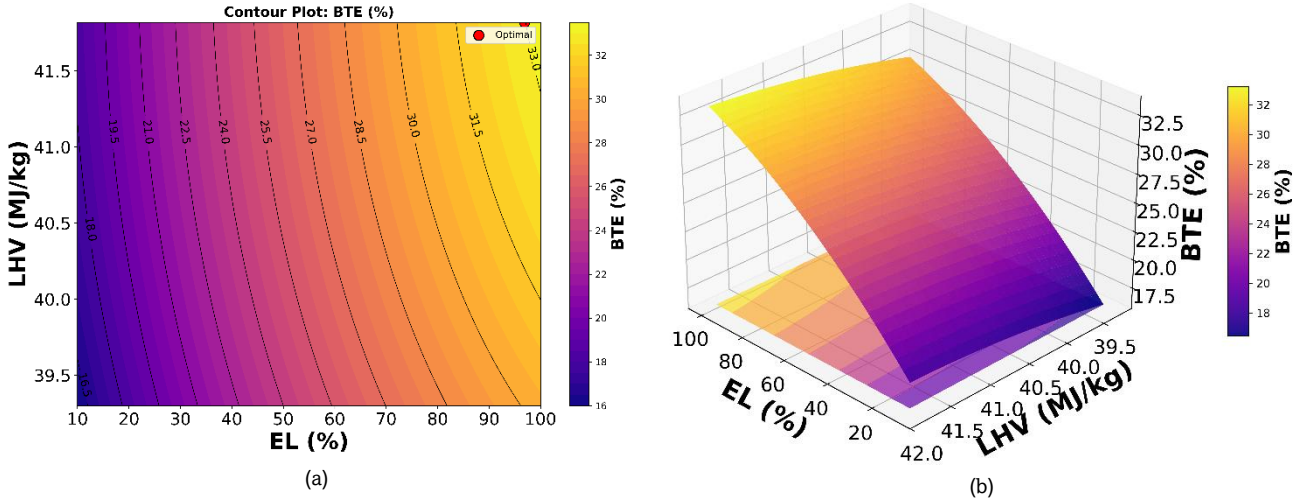

Fig 3. BTE model (a) contour plot (b) surface diagram

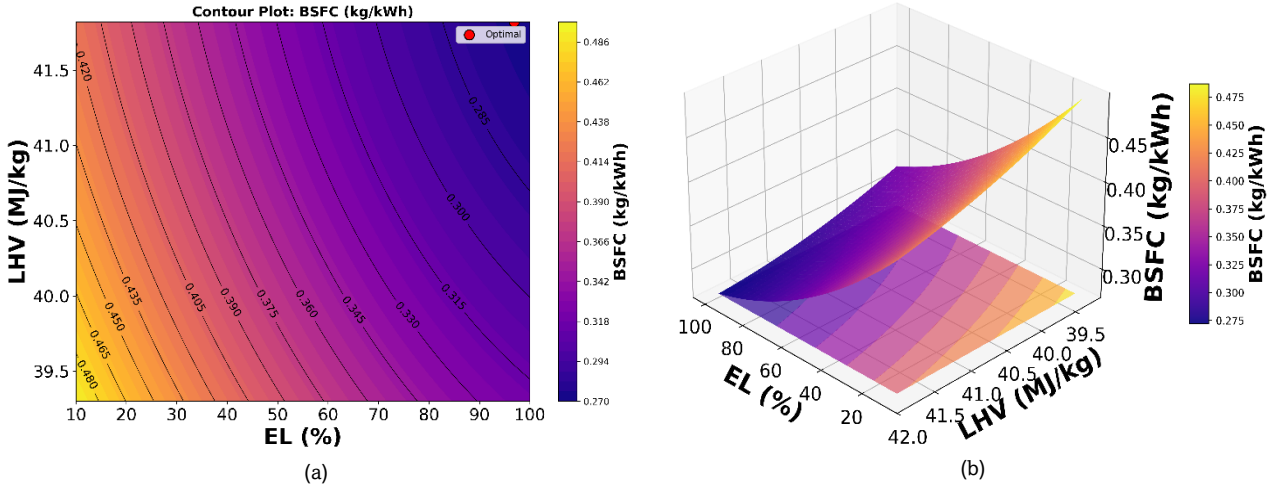

Fig 4. BSFCE model (a) contour plot (b) surface diagram

losses increase, and there may be combustion inefficiencies at extreme conditions.

3.2.2 Brake-specific fuel consumption model

Conversely, Fig. 4a and Fig. 4b show the opposite trend of B SFC, which is thermodynamically related to efficiency. Fig. 4a indicates that the contour plot indicates that BSFC declines considerably as EL increases, falling between 0.48 and 0.50 kg/kWh at low EL of 10% to about 0.28 and 0.30 kg/kWh at high EL of about 100%. This drastic decrease indicates better fuel consumption at high loads because of more efficient combustion and lower relative energy losses. The effect of LHV is once again indirect but observable with the BSFC decreasing between approximately 0.34 and 0.30 kg/kWh as the LHV increases between approximately 39.5 MJ/kg and 42 MJ/kg at an intermediate EL of 60% as the energy content of the fuel decreases. The gradient of EL is greater than LHV, as shown by the contour spacing, which is in line with the predominant role of load. This behavior is further explained in Fig. 4b, in which the 3D surface slopes steeper as EL increases and less steep as LHV increases. The maximum BSFC values of approximately 0.47-0.49 kg/kWh are at low EL and low LHV, and the minimum values of approximately 0.27-0.29 kg/kWh are at high EL and high LHV. The slight curvature of the surface indicates nonlinear interactions, especially at low EL, where inefficiencies are more significant. In general, both characters are able to show that EL is the main thermodynamic behavior of the system, and LHV is the secondary improvement, and the best performance is observed under high EL and high LHV conditions.

3.2.3 Oxides of nitrogen emission model

Fig. 5 to Fig. 7 show the change of NOx, CO, and HC emissions with EL and LHV using contour and surface plots, which clearly show that the formation of emissions is controlled by combustion temperature, oxidation completeness, and mixture characteristics. Fig. 5a is a contour plot of NOx, which demonstrates a steep upward trend with EL, with the values increasing between 300-350 ppm at low EL near 10 percent to almost 700-750 ppm at high EL near 100 percent. This sharp slope on the EL axis proves that load is the most important parameter that regulates the formation of NOx because the higher the EL is, the higher the temperature in the in-cylinder and the availability of oxygen, which facilitates the formation of thermal nitrogen oxide. NOx also rises more moderately along

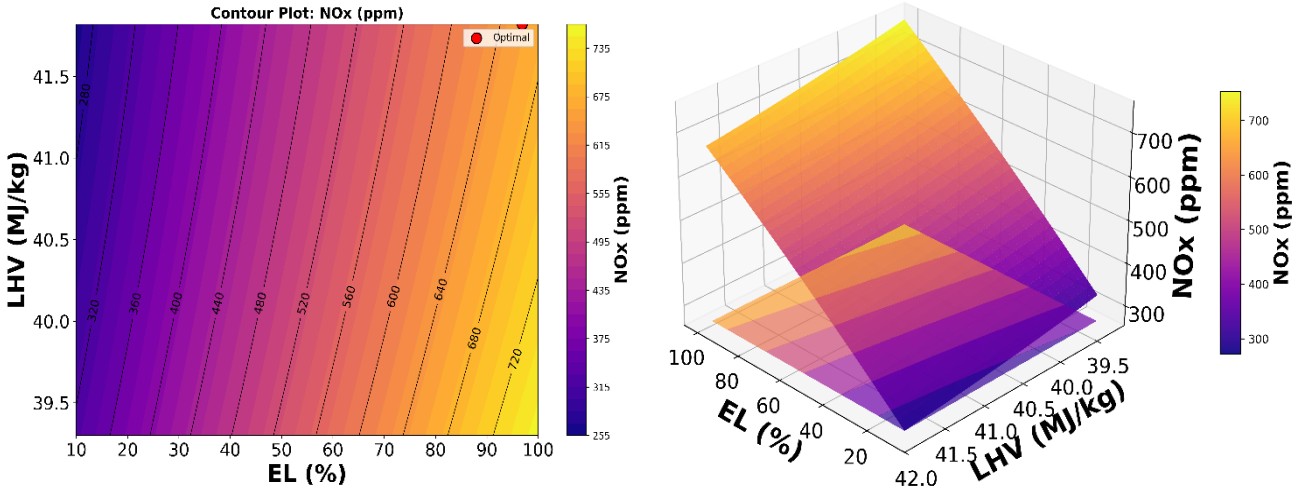

Fig 5. NOx emission model (a) contour plot (b) surface diagram

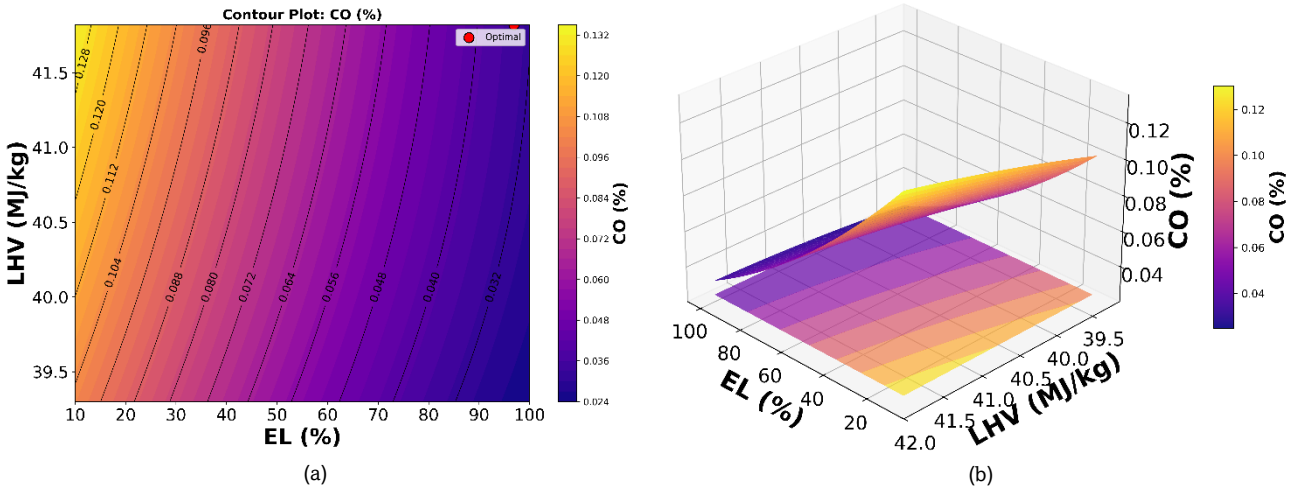

Fig 6. CO emission model (a) contour plot (b) surface diagram

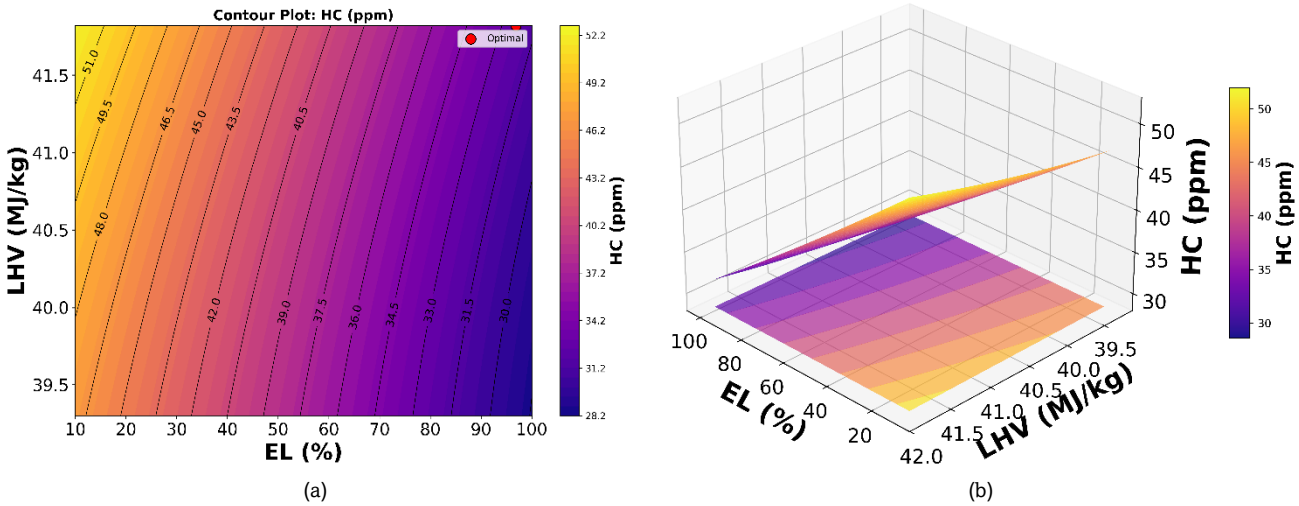

Fig 7. HC emission model (a) contour plot (b) surface diagram

the LHV axis, e.g., between approximately 450 and 600 ppm at 39.5 MJ/kg to almost 550-600 ppm at 41.5-42 MJ/kg at EL of approximately 60, meaning that increased fuel energy content raises flame temperature and increases NOx formation. The lines of contour are almost parallel, implying a linear dependence. This is further supported by Fig. 5b, which

indicates a smooth upward surface with maximum NOx values of more than 700 ppm at high EL and high LHV with little curvature, which implies weak nonlinear interaction.

3.2.4. Carbon monoxide emission model

Conversely, Fig. 6 shows the CO emissions, which have a reverse trend because they are generated during incomplete combustion. Fig. 6a shows that CO decreases considerably with EL, falling between 0.11-0.12% at low EL of 10% to about 0.04-0.05% at high EL of close to 100%. This shows that increased load enhances combustion completeness through increased temperature and oxidation rates, and thus, decreased CO formation. CO also declines a little along the LHV axis, e.g., between approximately 0.08% at 39.5 MJ/kg and almost 0.06% at 42 MJ/kg in EL at about 50%, indicating better combustion efficiency with higher energy content fuels. The gradient of the contour lines is steeper along EL than LHV, which proves the prevailing effect of load. Fig. 6b depicts a downward sloping surface with the maximum CO values at low EL and low LHV and minimum values at high EL and high LHV with slight curvature due to weak interaction effects.

3.2.5. Hydrocarbon emission model

Fig. 7 shows HC emissions, which are also due to incomplete combustion, unburned fuel pockets, and quenching effects. Fig. 7a shows that HC reduces significantly with EL, with a range of about 48-52 ppm at low EL (near 10 percent) and 30-32 ppm at high EL (near 100 percent). This tendency indicates enhanced flame propagation and oxidation at increased loads, minimizing HC emission formation (Hoang, 2019). HC also exhibits a moderate decline along the LHV axis, e.g., between approximately 40 ppm at 39.5 MJ/kg to approximately 34-36 ppm at 42 MJ/kg in the case of mid-range EL, which means that higher LHV favors better combustion conditions. The contour lines are slightly curved, indicating nonlinear effects at lower EL, where quenching and incomplete combustion are more dominant. This behavior is confirmed in Fig. 7b, where the surface decreases with increasing EL and LHV, and the highest values of HC are at low EL and low LHV. All in all, the emission plots show a consistent pattern of EL being the main controlling factor, followed by LHV, and that the higher the EL and LHV conditions, the lower the CO and HC, but the higher the NOx, because of the high combustion temperatures.

3.3 Desirability-based optimization

Fig. 8 builds on the analysis by quantifying the multi-objective trade-offs between performance and emissions in terms of Pareto optimization and desirability functions. Fig. 8 shows clearly that the Pareto front is a thermodynamic conflict between the brake thermal efficiency and the brake specific fuel consumption. With a rise in BTE of about 16 to 18% to about 32 to 33%, BSFC also declines by almost 0.4950 kg/kWh to 0.2728 kg/kWh, creating a clear inverse curve. This tendency is a manifestation of the basic correlation according to which the higher the efficiency of combustion, the less fuel is needed per unit of power output. The spacing of points on the curve implies a continuous solution space, and the smooth monotonic form implies predictable and stable behavior of the system. The marked optimal point is close to the lower efficiency region, approximately 17% BTE and 0.49 kg/kWh BSFC, meaning that when all the objectives, such as emissions, are optimized

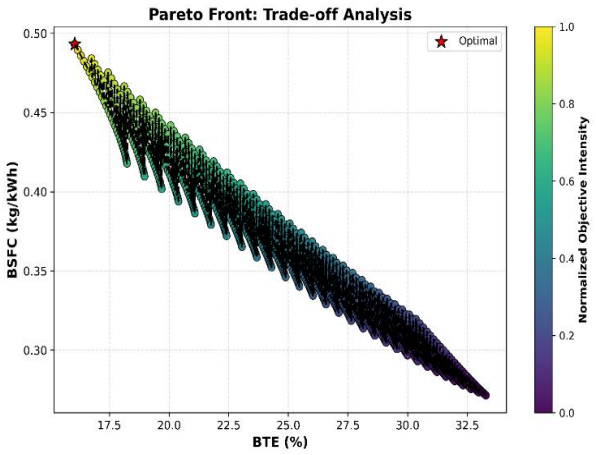

Fig. 8. Pareto chart

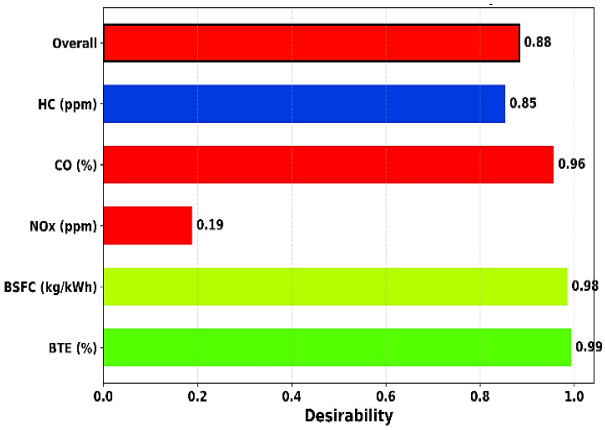

Fig 9. Desirability plot

simultaneously, the solution moves out of the purely efficiency-driven conditions. This is because the high BTE regions, though good in terms of fuel economy, are linked to high NOx emissions owing to high combustion temperatures, and the optimization has to trade off.

A more detailed interpretation is given in Fig. 9 in terms of individual and overall desirability values. BTE and BSFC have very high scores of desirability of 0.99 and 0.98, respectively, which means that the chosen optimal condition is almost at the highest possible performance targets of efficiency and fuel consumption within the given limits. The desirability of CO is also high (0.96), indicating that under the selected conditions, incomplete combustion is practically reduced. HC is slightly less desirable with a 0.85 value, indicating moderate but satisfactory amounts of unburned hydrocarbons. Conversely, NOx has a very low desirability of just 0.19, indicating the challenge of controlling thermal NO formation and maintaining high combustion efficiency.

The total desirability of 0.88 is a fair trade-off, with the majority of the responses being maximized except NOx, which is the constraint. This is in line with the physics of combustion, in which minimizing NOx is usually achieved by minimizing peak temperatures, at the cost of efficiency and full combustion. Collectively, these numbers indicate that although high EL and LHV are more inclined to performance indicators, a multi-objective optimization model is necessary to find a feasible operating point that can balance efficiency, fuel consumption, and emissions. The engine is working under peak thermal conditions at EL = 96.90% and LHV = 41.82 MJ/kg, with a high

BTE = 32.98% and low BSFC = 0.27 kg/kWh, which confirms that the engine is efficiently converting fuel energy into useful work. The increased load raises in-cylinder temperature and pressure, improving combustion completeness, as indicated by very low CO (0.03%) and HC (32.40 ppm). Nevertheless, the same temperature increase facilitates the formation of thermal NO, which leads to high levels of NOx emissions of 657.74 ppm. Therefore, the outcome is a typical trade-off in which better efficiency and lower incomplete combustion emissions are achieved at the cost of increased NOx because of increased combustion temperatures.

6. Conclusion

The current research paper develops a holistic connection between ultrasonic-aided production of biodiesel and optimization at the engine level through response surface methodology. The ultrasonic irradiation two-step transesterification process produced high-quality tobacco seed oil methyl ester that can be used in the engine. Both experimental and statistical evidence show that the most significant parameter that affects performance and emissions is engine load. One of the most interesting findings of the study is the determination of the peak operating conditions with EL = 96.90% and LHV = 41.82 MJ/kg, where the engine is most efficient with BTE = 32.98% and minimum fuel consumption of BSFC = 0.27 kg/kWh. These findings suggest very efficient combustion due to high in-cylinder temperature and pressure. Completeness of combustion is greatly enhanced at this condition, as indicated by very low CO (0.03%) and HC (32.40 ppm) emissions. The higher cylinder temperature also favors the formation of thermal NO, which leads to higher emissions of NOx of 657.74 ppm. The research contributes to the existing literature by performing a simultaneous analysis of several blend ratios and different loads and capturing the effects of interaction. Future efforts should be directed towards reducing NOx by using methods like exhaust gas recirculation, water injection, or post-treatment. Application of this framework to other non-edible biodiesels and real-world engine conditions will further increase its practical usefulness.

References

Ahmad, A., Yadav, A. K., & Dewangan, A. K. (2025). Synergistic effect of various nanoparticles infused biodiesel/diesel blends on combustion, performance, and environmental characteristics of a CI engine. *Journal of the Energy Institute*, *120*, 102117. https://doi.org/10.1016/j.joei.2025.102117

Ahmad, A., Yadav, A. K., Singh, A., Singh, D. K., & Ağbulut, Ü. (2024). A hybrid RSM-GA-PSO approach on optimization of process intensification of linseed biodiesel synthesis using an ultrasonic reactor: Enhancing biodiesel properties and engine characteristics with ternary fuel blends. *Energy*, *288*, 129077. https://doi.org/10.1016/j.energy.2023.129077

Alsaadi, S., Shakir, M. A., & Ahmad, M. I. (2025). A Comparative Review of Vegetative and Animal-Based Biodiesel: Feedstock Selection, Synthesis Method, Characterization Technique, and Economic Perspective. *Journal of Climate Change*, *11*(2), 22. https://doi.org/10.70917/jcc-2025-013

Awogbemi, O., Inambao, F., & Onuh, E. I. (2020). Optimization of FAME composition for improved engine performance and emissions reduction. *International Journal of Low-Carbon Technologies*, *15*(4), 583–593. https://doi.org/10.1093/ijlct/ctaa027

Chamkalani, A., Zendehboudi, S., Rezaei, N., & Hawboldt, K. (2020). A critical review on life cycle analysis of algae biodiesel: current challenges and future prospects. *Renewable and Sustainable Energy Reviews*, *134*, 110143. https://doi.org/10.1016/j.rser.2020.110143

Christopher Selvam, D., Devarajan, Y., & Raja, T. (2026). Biodiesel and alcohol-biodiesel blends in marine diesel engines: Fuel properties, engine behavior, environmental impacts, and operational challenges. *Marine Pollution Bulletin*, *224*, 119169. https://doi.org/10.1016/j.marpolbul.2025.119169

Desniorita, Permadani, R. L., Youfa, R., Nirmala, D., Pelita, E., Sahaq, A. B., & Jayanti, R. T. (2026). Optimization of Biodiesel Synthesis from Refined Bleached Deodorized Palm Oil Using Limestone CaO Catalyst Supported Chemically Activated Palm Oil Mill Fly Ash. *International Journal on Advanced Science, Engineering and Information Technology*, *16*(1), 101–109. https://doi.org/10.18517/ijaseit.16.1.21565

Di, Y., Cheung, C. S., & Huang, Z. (2009). Experimental investigation on regulated and unregulated emissions of a diesel engine fueled with ultra-low sulfur diesel fuel blended with biodiesel from waste cooking oil. *Science of The Total Environment*, *407*(2), 835–846. https://doi.org/10.1016/j.scitotenv.2008.09.023

Djimtoingar, S. S., Derkyi, N. S. A., Kuranchie, F. A., & Yankyera, J. K. (2022). A review of response surface methodology for biogas process optimization. *Cogent Engineering*, *9*(1). https://doi.org/10.1080/23311916.2022.2115283

Donatus Setyawan Purwo Handoko. (2022). Utilization of Waste Tobacco (Nicotiana Tabacum) Post-Harvest as an Alternative Biodiesel. *Jurnal Multidisiplin Madani*, *2*(12), 4343–4349. https://doi.org/10.55927/mudima.v2i12.1780

Dong, V. H., & Sharma, P. (2023). Optimized conversion of waste vegetable oil to biofuel with Meta heuristic methods and design of experiments. *Journal of Emerging Science and Engineering*, *1*(1), 22–28. https://doi.org/10.61435/jese.2023.4

Fornasier, F., Gomez, J. F. C., Sansone, F. D. C., Schneider, R. D. C. de S., Costa, A. B. da, Moraes, J. A. R., & Bravo, C. A. G. (2018). Biodiesel production from energy tobacco. *Orbital: The Electronic Journal of Chemistry*, *10*(2). https://doi.org/10.17807/orbital.v10i2.1120

Gang, W., Yuan, Y., Jiang, G., Guo, H., & Zhang, Z. (2025). Experimental Study on Combustion and Vibration Characteristics of Low-Speed Marine Diesel Engine Fuelled with Biodiesel. *Polish Maritime Research*, *32*(3), 154–162. https://doi.org/10.2478/pomr-2025-0043

Gunst, R. F., Myers, R. H., & Montgomery, D. C. (1996). Response Surface Methodology: Process and Product Optimization Using Designed Experiments. *Technometrics*, *38*(3), 285. https://doi.org/10.2307/1270613

Hoang, A. T. (2019). Experimental study on spray and emission characteristics of a diesel engine fueled with preheated bio-oils and diesel fuel. *Energy*, *171*, 795–808. https://doi.org/10.1016/j.energy.2019.01.076

Hoang, A. T. (2021). Prediction of the density and viscosity of biodiesel and the influence of biodiesel properties on a diesel engine fuel supply system. *Journal of Marine Engineering & Technology*, *20*(5), 299–311. https://doi.org/10.1080/20464177.2018.1532734

Hoang, A. T., Bora, B. J., Huynh, D. N. L., Nguyen, D. K. P., & Le, V. V. (2025). Dual-fuel diesel engine features powered by ammonia under various pilot-fuel injection timing: Comprehensive analysis and response surface methodology-based optimization. *International Journal of Engine Research*. https://doi.org/10.1177/14680874251341036

Hoang, A. T., Chen, W.-H., Paramasivam, P., Kanti, P. K., Huynh, D. N. L., Abdou El-Shafay, A. S., & Nguyen, V. Q. (2025). Comprehensive investigation on performance and emission of dual-fuel diesel engine fuelled with biodiesel and hydrogen using D-optimal design and desirability-based multi-attribute optimization. *International Journal of Hydrogen Energy*, *146*, 150005. https://doi.org/10.1016/j.ijhydene.2025.06.195

Hoang, A. T., Nayak, S. K., Vujanović, M., Guerrero-Pérez, M. O., Rodríguez-Castellón, E., López-Escalante, M. C., Ahmed, S. F., Hadiyanto, H., Luu, V. C., Nguyen, V. N., Nguyen, X. P., & Cao, D. N. (2025). Towards Sustainable Development Goals: Application of Hydrogen-Enriched Mahua Biodiesel/Diesel Blend to Dual-Fuel Diesel Engine. *Global Challenges*, *9*(10). https://doi.org/10.1002/gch2.202500260

Huynh, D. N. L., Hoang, A. T., Nayak, S. K., Guerrero-Pérez, M. O., Rodríguez-Castellón, E., López-Escalante, M. C., Sănduleac, M., Efremov, C., Bui, V. G., Luu, V. C., Nguyen, X. P., & Cao, D. N. (2025). Combining Babool wood-derived producer gas and hydrogen with biodiesel as efficient strategies for dual-fuel diesel

engine in advancing sustainable energy. *Case Studies in Thermal Engineering*, *75*, 107097. https://doi.org/10.1016/J.CSITE.2025.107097

John, C. B., J., G. J., & Baskar, S. (2026). A comprehensive evaluation of the impact of compression ratio on performance, combustion, and emissions of hemp biodiesel-fueled direct injection diesel engine. *Fuel*, *405*, 136627. https://doi.org/10.1016/j.fuel.2025.136627

Kalyani, T., Prasad, L. S. V., & Kolakoti, A. (2023). Biodiesel Production from a Naturally Grown Green Algae Spirogyra Using Heterogeneous Catalyst: An Approach to RSM Optimization Technique. *International Journal of Renewable Energy Development*, *12*(2), 300–312. https://doi.org/10.14710/ijred.2023.50065

Khandal, S. V., Razak, A., Veza, I., Afzal, A., Alwetaishi, M., Shaik, S., Ağbulut, Ü., & Rashedi, A. (2024). Hydrogen and dual fuel mode performing in engine with different combustion chamber shapes: Modelling and analysis using RSM-ANN technique. *International Journal of Hydrogen Energy*, *52*, 973–1005. https://doi.org/10.1016/j.ijhydene.2022.09.193

Kline, S. J., & McClintock, F. A. (1953). Describing Uncertainties in Single-Sample Experiments. *Mechanical Engineering*, *75*(1), 3–8. http://54.243.252.9/engr-1330-webroot/6-Projects/P-InstrumentCalibration/Kline_McClintock1953.pdf

Kober, T., Schiffer, H.-W., Densing, M., & Panos, E. (2020). Global energy perspectives to 2060 – WEC's World Energy Scenarios 2019. *Energy Strategy Reviews*, *31*, 100523. https://doi.org/10.1016/j.esr.2020.100523

Kolakoti, A., Setiyo, M., & Rochman, M. L. (2022). A Green Heterogeneous Catalyst Production and Characterization for Biodiesel Production using RSM and ANN Approach. *International Journal of Renewable Energy Development*, *11*(3), 703–712. https://doi.org/10.14710/ijred.2022.43627

Kuppuswami, S. B., Muthuswamy, P., Sekar, P., Chandrasekharan, T., Pavan, M., & Riyaz, S. (2024). Optimization of diesel engine - Performance and emission parameters utilizing RSM approach using biodiesel-diesel blends and compression. *Biopolymer, Smart Materials and Engineering Materials*, 020020. https://doi.org/10.1063/5.0194191

Le, K. B., Tran, M. P., & Cao, D. N. (2026). Hybrid Response Surface Methodology–Extreme Gradient Boosting Optimization of a Hemp Biodiesel–Diesel Fueled Compression Ignition Engine. *International Journal on Advanced Science, Engineering and Information Technology*, *16*(2), 372–384. https://doi.org/10.18517/ijaseit.16.2.14077

Le, T. T., Sharma, P., Osman, S. M., Dzida, M., Nguyen, P. Q. P., Tran, M. H., Cao, D. N., & Tran, V. D. (2024). Forecasting energy consumption and carbon dioxide emission of Vietnam by prognostic models based on explainable machine learning and time series. *Clean Technologies and Environmental Policy*, *26*(12), 4405–4431. https://doi.org/10.1007/s10098-024-02852-9

Lv, J., Sun, Y., Zhang, Z., & Fang, Y. (2024). Optimization of operational parameters of marine methanol dual-fuel engine based on RSM-MOPSO. *Process Safety and Environmental Protection*, *191*, 2634–2652. https://doi.org/10.1016/j.psep.2024.10.006

Mujtaba, M. A., Masjuki, H. H., Kalam, M. A., Ong, H. C., Gul, M., Farooq, M., Soudagar, M. E. M., Ahmed, W., Harith, M. H., & Yusoff, M. N. A. M. (2020). Ultrasound-assisted process optimization and tribological characteristics of biodiesel from palm-sesame oil via response surface methodology and extreme learning machine - Cuckoo search. *Renewable Energy*, *158*, 202–214. https://doi.org/10.1016/j.renene.2020.05.158

Muniyappan, S., & Krishnaiah, R. (2025). Optimizing engine operating parameters for enhanced performance in a combustion-enhanced ternary-fuelled compression ignition engine. *Scientific Reports*, *15*(1), 22611. https://doi.org/10.1038/s41598-025-05628-3

Naseef, H. H., & Tulaimat, R. H. (2025). Transesterification and esterification for biodiesel production: A comprehensive review of catalysts and palm oil feedstocks. *Energy Conversion and Management: X*, *26*, 100931. https://doi.org/10.1016/j.ecmx.2025.100931

Nayak, S. K., Nižetić, S., Pham, V. V., Huang, Z., Ölçer, A. I., Bui, V. G., Wattanavichien, K., & Hoang, A. T. (2022). Influence of injection timing on performance and combustion characteristics of compression ignition engine working on quaternary blends of diesel fuel, mixed biodiesel, and t-butyl peroxide. *Journal of Cleaner Production*, *333*, 130160. https://doi.org/10.1016/j.jclepro.2021.130160

Nguyen, D., Chau, T. H., Nguyen, D. C., Nguyen, D. T., & Nguyen, T. B. N. (2025). Artificial Intelligence and Machine Learning in Renewable Energy: From Prediction to Intelligent Optimization. *JOIV : International Journal on Informatics Visualization*, *9*(6), 2528. https://doi.org/10.62527/joiv.9.6.4889

Nguyen, T. H., Paramasivam, P., Dong, V. H., Le, H. C., & Nguyen, D. C. (2024). Harnessing a Better Future: Exploring AI and ML Applications in Renewable Energy. *JOIV : International Journal on Informatics Visualization*, *8*(1), 55. https://doi.org/10.62527/joiv.8.1.2637

Nguyen, V. G., Sharma, P., Dzida, M., Bui, V. H., Le, H. S., El-Shafay, A. S., Le, H. C., Le, D. T. N., & Tran, V. D. (2024). A Review on Metal–Organic Framework as a Promising Catalyst for Biodiesel Production. *Energy & Fuels*, *38*(4), 2654–2689. https://doi.org/10.1021/acs.energyfuels.3c04203

Nguyen, V. N., Sharma, P., Kumar, A., Pham, M. T., Le, H. C., Truong, T. H., & Cao, D. N. (2023). Optimization of biodiesel production from Nahar oil using Box-Behnken design, ANOVA and grey wolf optimizer. *International Journal of Renewable Energy Development*, *12*(4), 711–719. https://doi.org/10.14710/ijred.2023.54941

Onokwai, A. O., Akuru, U. B., & Desai, D. A. (2025). Predictive accuracy and characterisation of bio-oil yield from pyrolysis of Cocos nucifera: A comparison of traditional RSM and hybrid models. *International Journal of Renewable Energy Development*. https://doi.org/10.61435/ijred.2025.61190

Ouchikh, S., Lounici, M. S., Loubar, K., & Tazerout, M. (2025). Optimization of Injection Strategy for CH4/Diesel Dual-Fuel Engine Using Response Surface Methodology. *Energies*, *18*(8), 2115. https://doi.org/10.3390/en18082115

Oza, S., Prajapati, N., Kodgire, P., & Kachhwaha, S. S. (2021). An ultrasound-assisted process for the optimization of biodiesel production from waste cottonseed cooking oil using response surface methodology. *Water-Energy Nexus*, *4*, 187–198. https://doi.org/10.1016/j.wen.2021.11.001

Paramasivama, P., Naima, K., & Dzida, M. (2024). Soft computing-based modelling and optimization of NOx emission from a variable compression ratio diesel engine. *Journal of Emerging Science and Engineering*, *2*(2), e21. https://doi.org/10.61435/jese.2024.e21

Prajapati, A. K., Mahajan, A., Jadhav, S. M., & Kumar, K. (2026). Fourth-generation (4G) biodiesel: Paving the way for a greener and sustainable energy future in emerging economies. *Renewable and Sustainable Energy Reviews*, *225*, 116103. https://doi.org/10.1016/j.rser.2025.116103

Prakash Maran, J., & Priya, B. (2015). Modeling of ultrasound assisted intensification of biodiesel production from neem (Azadirachta indica) oil using response surface methodology and artificial neural network. *Fuel*, *143*, 262–267. https://doi.org/10.1016/j.fuel.2014.11.058

Quaranta, E., Dibenedetto, A., Colucci, A., & Cornacchia, D. (2022). Partial hydrogenation of FAMEs with high content of C18:2 dienes. Selective hydrogenation of tobacco seed oil-derived biodiesel. *Fuel*, *326*, 125030. https://doi.org/10.1016/j.fuel.2022.125030

Rahman, M., Kabir, S., Mustafi, N. N., & Robin, H. M. (2026). Effects of CeO2 nanoparticle additive in sesame seed biodiesel-diesel fuel blends on the performance of a diesel engine and emissions. *Next Research*, *4*, 101201. https://doi.org/10.1016/j.nexres.2025.101201

Rajak, U., Apparao, K. C., Verma, T. N., & Ağbulut, Ü. (2024). Enhancing performance, and combustion efficiency, and reducing tailpipe emissions of an engine fuelled with hydrogen-enriched diesel and ethanol blends at varying CRs using RSM. *International Journal of Hydrogen Energy*, *92*, 1236–1247. https://doi.org/10.1016/j.ijhydene.2024.10.289

Riayatsyah, T. M. I., Thaib, R., Silitonga, A. S., Milano, J., Shamsuddin, A. H., Sebayang, A. H., Rahmawaty, Sutrisno, J., & Mahlia, T. M. I. (2021). Biodiesel Production from Reutealis trisperma Oil Using Conventional and Ultrasonication through Esterification and Transesterification. *Sustainability*, *13*(6), 3350.

https://doi.org/10.3390/su13063350
Sakthivel, R., Ramesh, K., Purnachandran, R., & Mohamed Shameer, P. (2018). A review on the properties, performance and emission aspects of the third generation biodiesels. *Renewable and Sustainable Energy Reviews*, *82*, 2970–2992. https://doi.org/10.1016/j.rser.2017.10.037
Sarabia, L. A., & Ortiz, M. C. (2009). Response Surface Methodology. In *Comprehensive Chemometrics* (pp. 345–390). Elsevier. https://doi.org/10.1016/B978-044452701-1.00083-1
Sarve, A., Sonawane, S. S., & Varma, M. N. (2015). Ultrasound assisted biodiesel production from sesame (Sesamum indicum L.) oil using barium hydroxide as a heterogeneous catalyst: Comparative assessment of prediction abilities between response surface methodology (RSM) and artificial neural network (ANN). *Ultrasonics Sonochemistry*, *26*, 218–228. https://doi.org/10.1016/j.ultsonch.2015.01.013
Sebayang, A. H., Ideris, F., Silitonga, A. S., Shamsuddin, A. H., Zamri, M. F. M. A., Pulungan, M. A., Siahaan, S., Alfansury, M., Kusumo, F., & Milano, J. (2023). Optimization of ultrasound-assisted oil extraction from Carica candamarcensis; A potential Oleaginous tropical seed oil for biodiesel production. *Renewable Energy*, *211*, 434–444. https://doi.org/10.1016/j.renene.2023.04.099
Sebayang, A. H., Kusumo, F., Milano, J., Shamsuddin, A. H., Silitonga, A. S., Ideris, F., Siswantoro, J., Veza, I., Mofijur, M., & Reen Chia, S. (2023). Optimization of biodiesel production from rice bran oil by ultrasound and infrared radiation using ANN-GWO. *Fuel*, *346*, 128404. https://doi.org/10.1016/j.fuel.2023.128404
Shami, T. M., Summakieh, M. A., Alswaitti, M., Jahdhami, M. A. Al, Sheikh, A. M., & El-Saleh, A. A. (2023). TPPSO: A Novel Two-Phase Particle Swarm Optimization. *JOIV : International Journal on Informatics Visualization*, *7*(3–2), 2095. https://doi.org/10.30630/joiv.7.3-2.2331
Sharma, P., Chhillar, A., Said, Z., Huang, Z., Nguyen, V. N., Nguyen, P. Q. P., & Nguyen, X. P. (2022). Experimental investigations on efficiency and instability of combustion process in a diesel engine fueled with ternary blends of hydrogen peroxide additive/biodiesel/diesel. *Energy Sources, Part A: Recovery, Utilization, and Environmental Effects*, *44*(3), 5929–5950. https://doi.org/10.1080/15567036.2022.2091692
Sharma, P., & Sharma, A. K. (2022). Statistical and Continuous Wavelet Transformation-Based Analysis of Combustion Instabilities in a Biodiesel-Fueled Compression Ignition Engine. *Journal of Energy Resources Technology*, *144*(3). https://doi.org/10.1115/1.4051340
Shrivastava, K., Thipse, S. S., & Patil, I. D. (2021). Optimization of diesel engine performance and emission parameters of Karanja biodiesel-ethanol-diesel blends at optimized operating conditions. *Fuel*, *293*, 120451. https://doi.org/10.1016/j.fuel.2021.120451
Susaimanickam, A., Manickam, P., & Joseph, A. A. (2023). A Comprehensive Review on RSM-Coupled Optimization Techniques and Its Applications. *Archives of Computational Methods in Engineering*, *30*(8), 4831–4853. https://doi.org/10.1007/s11831-023-09963-4
Szulczyk, K. R., & Badeeb, R. A. (2022). Nontraditional sources for biodiesel production in Malaysia: The economic evaluation of hemp, jatropha, and kenaf biodiesel. *Renewable Energy*, *192*, 759–768. https://doi.org/10.1016/j.renene.2022.04.097
Teklehaimanot, H., Gupta, N., & Nallamothu, R. B. (2025). The impact of Al2O3 nano additives on Jatropha curcas biodiesel-diesel blend on combustion and emission behavior. *Energy Conversion and Management: X*, *25*, 100870. https://doi.org/10.1016/j.ecmx.2025.100870
Tian, Y., Liu, X., Fan, C., Li, T., Qin, H., Li, X., Chen, K., Zheng, Y., Chen, F., & Xu, Y. (2021). Enhancement of Tobacco (Nicotiana tabacum L.) Seed Lipid Content for Biodiesel Production by CRISPR-Cas9-Mediated Knockout of NtAn1. *Frontiers in Plant Science*, *11*. https://doi.org/10.3389/fpls.2020.599474
Ugraram, R. (2025). Performance optimization of oxy-fuel combustion diesel engine with EGR based on fuel injection parameters using response surface methodology (RSM). *Journal of Thermal Engineering*, 301–313. https://doi.org/10.14744/thermal.0000896
Usta, N., Aydoğan, B., Çon, A. H., Uğuzdoğan, E., & Özkal, S. G. (2011). Properties and quality verification of biodiesel produced from tobacco seed oil. *Energy Conversion and Management*, *52*(5), 2031–2039. https://doi.org/10.1016/j.enconman.2010.12.021
Veljković, V. B., Lakićević, S. H., Stamenković, O. S., Todorović, Z. B., & Lazić, M. L. (2006). Biodiesel production from tobacco (Nicotiana tabacum L.) seed oil with a high content of free fatty acids. *Fuel*, *85*(17–18), 2671–2675. https://doi.org/10.1016/j.fuel.2006.04.015
Vellaiyan, S. (2025). Enhancement of combustion performance and emission control in Bauhinia malabarica biodiesel-diesel blends using aluminium oxide nanoparticles and electrostatic precipitators. *Cleaner Engineering and Technology*, *26*, 100981. https://doi.org/10.1016/j.clet.2025.100981
Wan Osman, W. N. A., Rosli, M. H., Mazli, W. N. A., & Samsuri, S. (2024). Comparative review of biodiesel production and purification. *Carbon Capture Science & Technology*, *13*, 100264. https://doi.org/10.1016/j.ccst.2024.100264
Wei, C., Jiang, G., Wu, G., Zhou, Y., & Liu, Y. (2024). Effects on of Blended Biodiesel and Heavy Oil on Engine Combustion and Black Carbon Emissions of a Low-Speed Two-Stroke Engine. *Polish Maritime Research*, *31*(1), 94–101. https://doi.org/10.2478/pomr-2024-0010
Yew, G. Y., Lee, S. Y., Show, P. L., Tao, Y., Law, C. L., Nguyen, T. T. C., & Chang, J.-S. (2019). Recent advances in algae biodiesel production: From upstream cultivation to downstream processing. *Bioresource Technology Reports*, *7*, 100227. https://doi.org/10.1016/j.biteb.2019.100227
Zafar, M., Hussain, A., Ahmed, T., Daabo, A., & Ullah, F. (2026). Addition of Nanoparticles to Biodiesel–Diesel Blends to Improve Engine Efficiency and Reduce Tailpipe Emission. In *Machine Learning for Sustainable Energy Solutions* (pp. 139–159). Wiley. https://doi.org/10.1002/9781394267439.ch8
Zhang, W., Ou, J., Chen, Z., Li, Z., Zhijun, L., & Pan, M. (2025). Multi-objective performance optimization of diesel engine lip jet combustion chamber based on RSM-NSGA-Ⅱ. *Energy*, *330*, 136825. https://doi.org/10.1016/j.energy.2025.136825
Zullaikah, S., Putra, A. K., Fachrudin, F. H., Naulina, R. Y., Utami, S., Herminanto, R. P., Rachmaniah, O., & Ju, Y. H. (2021). Experimental Investigation and Optimization of Non-Catalytic In-Situ Biodiesel Production from Rice Bran Using Response Surface Methodology Historical Data Design. *International Journal of Renewable Energy Development*, *10*(4), 803–810. https://doi.org/10.14710/ijred.2021.34138